Synergistic Effect of Compatibilizer in Organo-Modified Layered Silicate Reinforced Butadiene Rubber Nanocomposites

Wei-Gwo Hwang, Kung-Hwa Wei
Department of Materials Science and Engineering, National Chiao Tung University, Hsinchu, Taiwan 30049, Republic of China

Chang-Mou Wu
Department of Environmental Resources Management, Applied Science and Technology Research Center, Transworld Institute of Technology, Yunlin, Taiwan 64063, Republic of China

We have prepared nanocomposites of intercalated and exfoliated organosilicates in butadiene rubber (BR) by using a two-stage melt blending process. We used X-ray diffraction and transmission electron microscopy to examine, respectively, the intergallery spacing of the organosilicates and their dispersion in the BR. Marked enhancements in the mechanical and thermal properties of BR occurred when it incorporated <10 parts of organosilicates and the loading ratio of the organosilicate to dicarboxylic acid-terminated butadiene oligomer was approximately three. In particular, the addition of 10 parts of organosilicate and 3 parts of compatibilizer in the BR led to a more than four-fold increase in the tensile strength, a 150% increase in modulus at 100% elongation (M100), and 232 and 410% enhancements in the tear strength and elongation at break, respectively, relative to those of neat BR. The degradation temperature for the BR nanocomposite containing only a 10-part loading of organosilicate was 51°C higher than that of neat BR; these increases reduced, however, to 9–13°C upon the addition of the CTB compatibilizer. In addition, the relative water vapor permeabilities of the BR nanocomposites containing 10 parts of organosilicate—both in the presence and absence of the compatibilizer—reduced to 20% of that of the neat BR. POLYM. ENG. SCI., 46:80–88, 2006.

INTRODUCTION

Polymer nanocomposites based on the reinforcing of silicate layers derived from montmorillonite and thermoplastic or thermosetting polymers have been developed extensively over the past decade [1–5]. These materials have been predicted to provide superior mechanical strength, stiffness, thermal stability, and barrier properties, even when using only a very low weight percentage of montmorillonite [6–9]. Typically, an intercalated or exfoliated structure of the layered silicate can be obtained in the host polymer. Intercalated layered silicates possess a slightly increased intergallery space, which appears as an intense peak at a lower X-ray diffraction angle, and they retain their same orientation in the polymer matrix. In contrast, exfoliated silicates exist as monolayer silicates that become completely separated from one another in the polymer matrix; they are characterized by the absence of intense peaks in their XRD patterns, as well as through TEM observations.

Several methods have been developed for the effective preparation of intercalated or exfoliated layered silicate reinforced nanocomposites of nylon, polyimide, epoxy, polysiloxane, acrylonitrile butadiene rubber (NBR), SBR, polyurethane matrixes, and the other polymer systems [1–23]. These methods include in situ polymerization of monomers [7, 10–13], melt blending [14–18], emulsion polymerization or latex blending [19, 20], and solution blending using polar organic solvents [21–23]. In most cases, suitable chemical treatment and optimized processing are both keys to the successful formation of the nanocomposites. In our laboratory, we have obtained some nanocomposites that have potential for application in the electronics and dipped goods industries [7, 12, 19].

To obtain exfoliated nanocomposites, it is necessary to select amphiphilic molecules to modify the layered silicates, expand the intergallery space, and interact suitably with the molecules in the matrix. One end of the amphiphilic molecule may be, for example, a hydrophilic quaternary alkylammonium ion unit for interacting with the silicates, while

Correspondence to: Kung-Hwa Wei; e-mail: khwei@cc.nctu.edu.tw
Contract grant sponsor: Ministry of Economic Affairs through Project; contract grant number: 93FCAA0V; contract grant sponsor: National Science Council; contract grant number: NSC93–2623-7–009-014.
DOI 10.1002/pen.20450
Published online in Wiley InterScience (www.interscience.wiley.com).

the other end may have hydrophobic groups or chemically reactive functional groups that can be either compatible with or covalently bonded to the polymer, thereby increasing the miscibility of the silicates and the polymers [4, 24]. A suitable compatibilizing component can be used to increase the interaction of two originally immiscible surfaces through hydrogen bonds, to avoid phase separation and to prevent interfacial failure [25–30]. Polarity is the other significant factor to be considered when preparing a successful polymer nanocomposite. Organo-modified layered silicates having high polarity and largely expanded d-spacing are relatively easier to intercalate with a highly polar polymer when using a method such as shear blending, but they are not miscible with nonpolar polymers. Preparing a miscible and well-intercalated nanocomposite from a nonpolar polymer and a polar organosilicate usually requires a compatibilizer to act as a surfactant.

Carbon black and silica are the two most effective rubber reinforcing agents. In contrast, only a few studies have been reported on the use of organosilicates to reinforce rubber. For a conventional filling effect, the main factors that cause significant reinforcement are a high specific area, the nature of the structure, and the surface chemistry. The reinforcing effect of rubber nanocomposites containing just a few weight percent of layered silicates is similar to that of rubber compounds having much higher loadings of silica or carbon black [15, 31, 32]. The efficiency of the silicates in modifying the properties of the rubber is largely determined by their degree of dispersion and the extent of their exfoliation in the rubber. Polyolefinic rubbers are more hydrophobic than are a number of thermoplastics and, therefore, it is necessary to process the layered silicates properly to achieve good dispersion. In addition, the very high viscosity of molten rubber, due to its high molecular weight, can generate high shear stresses locally during compounding, and cause the peeling apart of layered silicate stacks. Therefore, the layered silicates will be much easier to be delaminated [33, 34]. In this study, we used a two-stage compounding procedure—high-shear-force blending in a Banbury mixer at room temperature followed by hot-melt blending at 150°C—along with the use of a selected compatibilizer to obtain the intercalated/delaminated rubber nanocomposites.

To obtain a more detailed expression on the reinforcing effect of the organosilicate in rubber, we selected a nonpolar butadiene rubber (BR) and a hydrophobic organosilicate to produce the nanocomposites through a two-stage melt blending method. Because BR is one of the most important industrial raw materials whose reinforcement has only a fewer to be reported [30, 35], we believed that such a study would be of great importance. In this study, we examined the effect that the amount of organosilicate has on the mechanical, thermal, and barrier properties of the resulting nanocomposites. In addition, we also studied the thermodynamic behavior of these nanocomposites.

TABLE 1. Formulation of BR/organosilicate nanocomposites.

Material	phr
BR, Taipol 0150	100
Organosilicate, Nanomer 1.28E	0–10 (various)
CTB	0–3
CTBN	0 or 3
ZnO	5
Stearic acid	2
Process aid	3.7
Sulfur	1.5
Accelerators	1.5

phr: Parts per hundred rubber.

EXPERIMENTAL

Material Preparation

Butadiene rubber (Taipol, BR, 0150, Taiwan Synthetic Rubber Co., Taiwan, R.O.C.), a conventional nonpolar material that has poor green strength and tear strength, was selected as the rubber matrix. Nanomer I.28E, an organosilicate modified by quaternary trimethylstearylammonium ions having an approximate aspect ratio of 75–120, was purchased from Nanocor Co., USA. The compatibilizers used in this study—carboxylated terminated butadiene oligomer (CTB) and carboxylated terminated butadiene acrylonitrile copolymer (CTBN) having a molecular weight of ~3000–4000 g/mol—were obtained from Aldrich Chemical Co., USA. Different contents of the layered silicates and compatibilizer were added to BR; they are named BR-0 (neat BR), BR-5 (BR having a loading of 5 wt% of layered silicates), and BR-5–7.5 (BR having a loading of 5 wt% layered silicates and a 7.5% weight ratio of CTB to the layered silicates). Typical industrial formulations were used (Table 1).

Process Design

The compounds of rubber/organosilicate nanocomposites were prepared in a 3-l Banbury mixer using a two-stage process. The first stage of the two-stage process involved blending the rubber, organosilicate, compatibilizer, and any other additives at room temperature in a Banbury mixer with the degree of fill at 80% and a rotation speed of 60 rpm for 8 min, then adding zinc oxide and blending again for 2 min before dropping down. The second stage involved reblending the compounds at 150°C in the mixer for 4 min with the similar mixing condition as the first stage, dropping down the compounds, then by adding the cure agents at room temperature on a two-mill roller. After aging at room temperature for 24 h, the samples were cured at 160°C in an electrically heated hydraulic press to their respective cure times, t_{90}. These values were derived from a Monsanto oscillating disc rheometer (MDR 2000)—-cf. Table 2. Then, the test specimens were prepared.

TABLE 2. Representative vulcanization characteristics of BR/organosilicate nanocomposites.

BR-(1.28E)-(ratio of CTB to 1.28E)	t_2 (s)	t_{90} (s)	M_L (lb in.)	M_R (lb in.)	$M_H - M_L$ (lb in.)
Neat BR	169	285	0.76	7.80	7.04
BR-10	81	160	0.89	8.10	7.21
BR-10–7.5	81	168	0.86	7.88	7.02
BR-10–15	82	168	0.81	7.70	6.89
BR-10–30	85	175	0.76	7.30	6.54
BR-10–45	84	175	0.72	6.77	6.05

t_2: Initial scorch time to 2 units of torque increase above minimum torque; t_{90}: cure time to 90% of maximum torque development; M_L: minimum torque; M_H: maximum equilibrium torque; $M_H - M_L$: torque increase.

Characterization

Tensile and tear tests were performed on a material testing system machine (Sintech, MTS, USA) at a cross-head speed of 50 cm/min, according to the ASTM standards D 412 and D 624, respectively. For each data point, five specimens were tested, and the average of the values was obtained. Thermogravimetric analysis (TGA) of each sample was performed under a nitrogen purge in a Perkin–Elmer TGA-7 instrument. The cured sample (~10 mg) was heated from 50 to 750°C at a rate of 10°C/min. Dynamic mechanical thermal analysis (DMA7, Perkin–Elmer) spectra were recorded using 6-cm-long, 1-cm-wide, and 0.25-cm-thick rectangular specimens in the tensile mode at a frequency of 10 Hz. DMTA spectra, viz. the storage modulus and mechanical loss factor (tan δ), were measured over the temperature range from −100 to 70°C at a heating rate of 5°C/min.

Wide-angle X-ray diffraction (XRD) patterns of the rubber samples were obtained using a D5000 diffractometer (Siemens, Munich, Germany) and Ni-filtered CuK_α radiation ($\lambda = 0.1542$ nm). The samples were scanned in the step mode at a scan rate of 1.5°/min in the range $2\theta < 10°$. Transmission electron microscopy (TEM) measurements were performed using a JEOL JEM 2000FX electron microscope operating at an acceleration voltage of 200 kV. Ultrathin sections of the cured samples were microtomed, using a Leica Ultracut Uct and a diamond knife, into ~100-nm-thick slices; subsequently, a layer of carbon was deposited onto these slices, and then, they were placed onto 400-mesh copper nets. Field emission scanning electron microscopy (FE-SEM) images were obtained using a JEOL JSM-6340F electron microscope operating at an acceleration voltage of 5 kV and 12.5 μA. A layer of gold was deposited onto the inspected section of the cured samples, using a JFC-1200 fine-coater. The water vapor permeability was measured using a Mocon PERMATRAN-W 3/60 instrument at 40°C and 90% relative humidity of water.

The crosslinking density was determined by performing equilibrium swelling as described in a previous report [31]. Swelling experiments were performed with the cured samples by equilibrating them in toluene at 25°C for 48 h. The uptake solvent percentage, Q, and volume fraction of BR in the swollen gel, Vr, were calculated using the following equations

$$Q = (M_{sw} - M_i)/M_i \tag{1}$$

where M_i and M_{sw} are the weights of the rubber sample before immersion in the solvent and in its swollen state, respectively.

$$Vr = (1/D_{sam})/[(1/D_{sam}) + (Q/D_{sol})] \tag{2}$$

where D_{sam} and D_{sol} are the densities of the rubber sample and solvent, respectively (0.87 for toluene). The crosslinking density of the sample, ν, defined by the number of elastically active chains per unit volume, was calculated by applying the Flory–Rehner equation [36]

$$\nu = -\frac{\ln(1-Vr) + Vr + \chi Vr^2}{Vs(Vr^{1/3} - Vr/2)} \tag{3}$$

where Vs is the molar volume of the swelling solvent (106.1 cm^3/mol for toluene) and χ is the Flory–Huggins (rubber–toluene) interaction parameter, which was taken to be 0.38 for the BR–toluene system. Determining the thermodynamic aspects of the rubber elasticity is crucial for obtaining a deeper understanding of the mixing in the BR/silicate nanocomposites. The expansion of rubber in the presence of a solvent will significantly modify the conformational entropy (ΔS) and the elastic Gibbs free energy (ΔG). The elastic Gibbs free energy can be determined from the Flory–Huggins equation [9, 14]

$$\Delta G = RT\,[\ln(1-Vr) + Vr + \chi Vr^2]. \tag{4}$$

From the statistical theory of rubber elasticity, the conformational entropy ΔS can be obtained from the equation $\Delta G = -T\Delta S$, which assumes that no changes in the internal energy of the network occur upon stretching.

RESULTS AND DISCUSSION

Vulcanization Property

Table 2 lists the representative vulcanization characteristics of BR nanocomposites containing 10 phr organosilicate and different amounts of compatibilizer. In the presence of organosilicates, the initial scorch time, t_2, was shorter than that of neat BR (81 vs. 169 s). This phenome-

 DOI 10.1002/pen

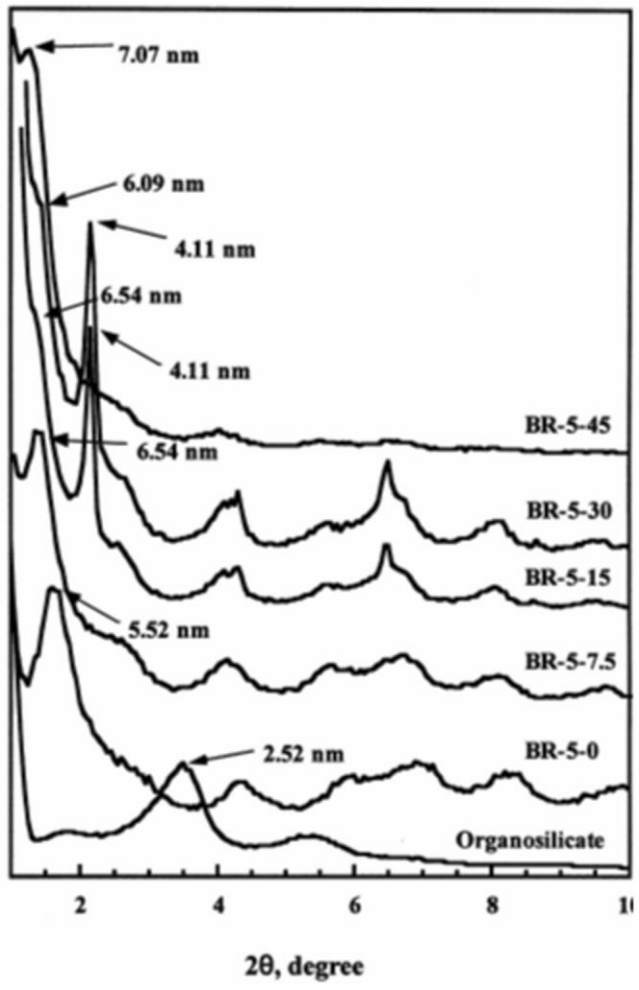

FIG. 1. XRD patterns of BR nanocomposites containing various contents of organosilicates.

non occurred because the acidic nature of the organosilicate activates the formation of soluble zinc ions, which in turn induces the decomposition of the accelerator into free radicals in an earlier stage of the reaction. These free radicals cause the premature vulcanization, which results in a decrease of the scorch time. The cure time, t_{90}, behaves in a manner similar to that of the t_2; this behavior is caused by a catalytic effect that has been reported previously [9]. Some accelerator free radicals for crosslinking can react with the compatibilizer and, therefore, retard the curing time. The values of both M_L and M_H of these nanocomposites increase upon the addition of the organosilicate at a low concentration; these increases result in an increase in the stiffness of the BR matrix based on the same curing system, but a decrease when the amount of compatibilizer increases. The increasing stiffness, $M_H - M_L$, follows the same trend as does the value of M_H.

Distribution and Dispersion of the Silicates

The efficiency of the organosilicate in reinforcing the polymer matrix is determined primarily by the degree of its dispersion in the matrix and by the extent in which the polymer molecules intercalate in the organosilicate. Figure 1 shows the XRD patterns of the representative BR nanocomposites containing 5 phr of organosilicate and various amounts of CTB. The pure organosilicate displays two independent diffraction peaks, denoted (001, A) and (001, B), having values of $2\theta \sim 3.51°$ ($d_{001,\ A} = 2.52$ nm) and 5.43° ($d_{001,\ B} = 2.63$ nm), respectively. The BR/organosilicate nanocomposites also display two independent diffraction peaks due to the addition of the organosilicate. The largest intercalated intergallery distance of these BR/organosilicate nanocomposites is much higher than that of the pure organosilicate ($d_{001,\ A} = 2.52$ nm). Table 3 lists the complete XRD data of the BR/organosilicate nanocomposites. The lowest diffraction peak of these nanocomposites, denoted (001, A), has values of 2θ between 1.2 and 1.8° ($d_{001,\ A} = 4.77$–7.07 nm). Another independent diffraction plane, denoted (001, B), has values of 2θ between 2.1 and 2.2° ($d_{001,\ B} = 4.01$–4.21 nm). The very clear multidiffraction peaks at ~4.2 and 6.5°, which result from higher-order diffraction, reflect the well-defined layered silicate structure. This observation indicates that, at a proper silicate loading and using a suitable mixing process, the viscosity of the nanocomposite can be large enough to generate a sufficient shearing force to further separate the intercalated silicate layers and to allow the rubber molecules to diffuse into the intergalleries, where the compatibilizers are miscible with the rubber molecules. As a result, the d-spacing of the layered silicate is expanded sufficiently. In the case of the 5 phr organosilicate in BR, a lower, but strong, peak appeared at ~6.5° (1.36 nm); this signal has been attributed to the thermal degradation and desorption of the organic materials in the gallery [37] or to an effect of the organosilicate confinement (reaggregation) [9, 14, 31]. The formation of a zinc–sulfur accelerator complex "extracts" the amine intercalant of the organosilicates, which, thus, causes the collapse of the layers.

TABLE 3. X-Ray diffraction data of BR/organosilicate nanocomposites.

BR-(1.28E)-(weight ratio of CTB to 1.28E)	001, A (nm)	001, B (nm)	002, B (nm)
Pure organosilicate	2.52	1.63	
BR-5	5.52	4.03	2.03
BR-5–7.5	6.54	4.17	2.16
BR-5–15	6.54	4.11	2.05
BR-5–30	6.09	4.11	2.05
BR-5–45	7.07	4.21	2.21
BR-7.5	6.09	4.02	2.08
BR-7.5–7.5	6.54	4.19	2.15
BR-7.5–15	6.31	4.01	2.08
BR-7.5–30	6.54	4.01	2.08
BR-7.5–45	6.54	4.21	2.15
BR-10	4.77	4.01	1.98
BR-10–7.5	5.70	4.15	2.13
BR-10–15	5.35	4.07	2.10
BR-10–30	5.89	4.11	2.08
BR-10–45	No peak	–	–

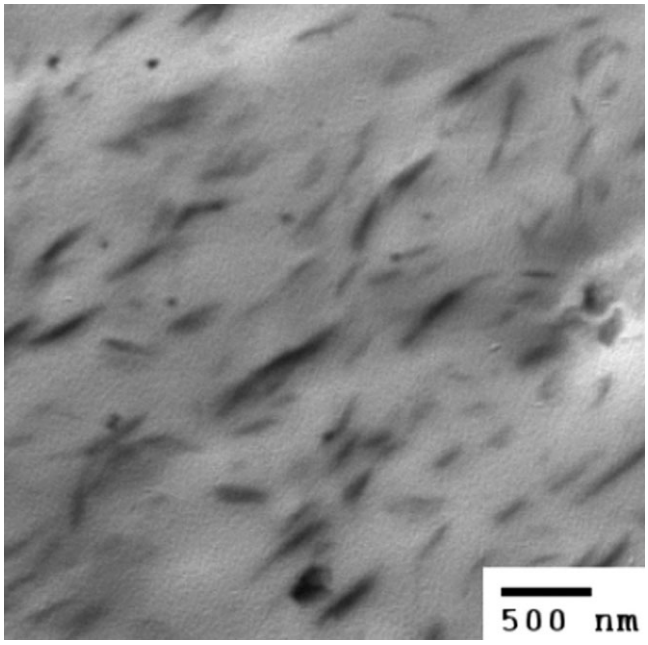

FIG. 2. TEM image of the BR nanocomposite containing 10 phr organosilicate and 3 phr CTB.

Figure 2 displays a TEM image of the BR nanocomposite containing 10 phr organosilicate and 3 phr CTB compatibilizer. Most of the layered silicates are dispersed well in the BR matrix, and a large portion of the organic-modified silicate layer particles appear to be intercalated along with a few single delaminated platelets. No visible differences appear in the morphology of the BR/organosilicate nanocomposites. Figure 3 presents an enlarged TEM

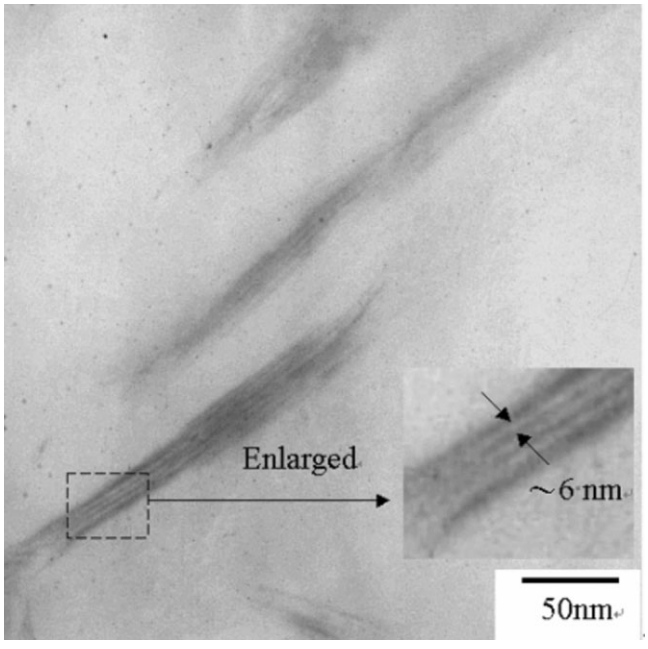

FIG. 3. Local enlarged TEM image of the BR nanocomposite containing 10 phr organosilicate and 3 phr CTB.

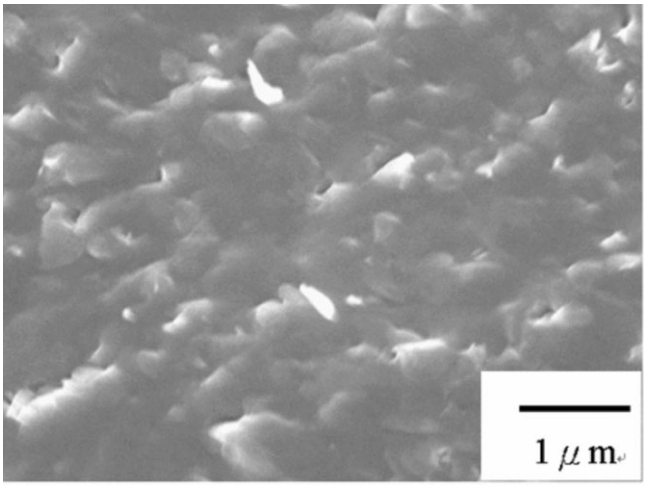

FIG. 4. FE-SEM image of the NBR nanocomposite containing 10 phr organosilicate and 3 phr CTB.

image. It is apparent that there are approximately four to seven layers of single intercalated platelets that have an intergallery distance of ~6 nm. Figure 3 indicates that the layered silicate bundles exist in the BR/organosilicate nanocomposite, which suggests an intercalated tactoids morphology. The results of TEM analysis are in consistent with those of an XRD study (Table 3). Thus, the TEM and XRD results both confirm that the layers of the organosilicate particles have become intercalated in the BR nanocomposites, and that the structures of the organosilicate platelets can be described as intercalated tactoids. At a high silicate loading, dispersion of layered silicates becomes difficult, but the high shear force applied causes the large rubber molecules to intercalate into the gallery of the layered silicates. This process may primarily contribute to the synergistic effect of the proper shear force and the wetting effect of the compatibilizer between the BR molecular chains and layered silicates. The well-understood wetting effect would result in the BR rubber molecule chains migrating or transporting into the largely expanded intergallery spaces of the layered silicates.

The influence that the compatibilizer has on the morphology of the BR/organosilicate nanocomposites can be visualized from the fractured surface. Compatibilizers usually act as wetting agents—improving the surface energy of both immiscible phases—that become entangled or interlocked with the bulk chains at the interface between the two incompatible components. It is sometimes necessary to connect a ductile rubber with a semirigid filler in a mechanical blending system through suitable selection of a compatibilizer, which increases the mechanical strength of the interface by allowing stress transfer to occur across it [25, 26, 28–30]. In our present system, which differs from that of a highly polar NBR [31], the compatibilizing effect is the dominant factor when the nonpolar BR incorporates the polar-structured organosilicates. Figures 4 and 5 display FE-SEM images of the fracture surfaces of the BR/organosilicate nanocomposites containing and lacking the compati-

 DOI 10.1002/pen

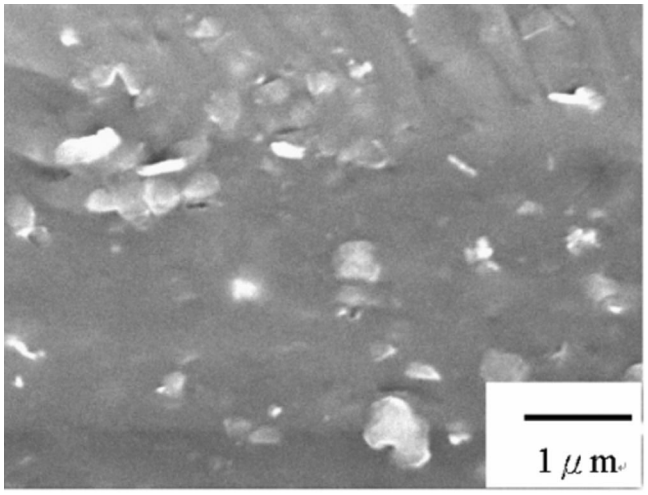

FIG. 5. FE-SEM image of the BR nanocomposite containing 10 phr organosilicate (without CTB).

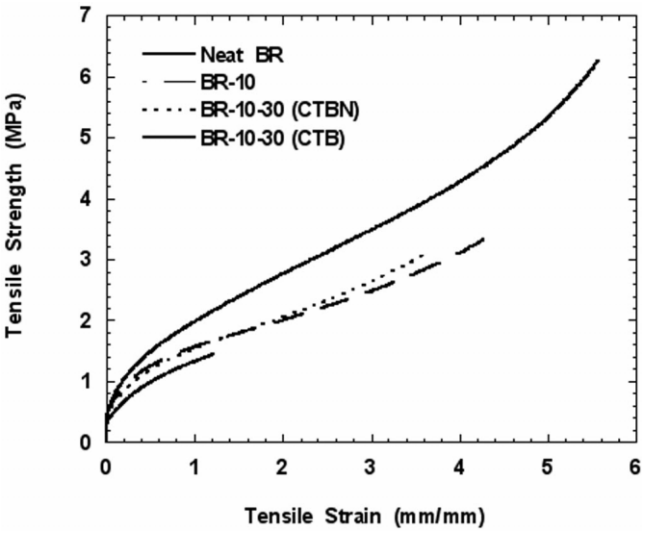

FIG. 6. Typical tensile stress–strain curves of the BR nanocomposites containing 10 phr organosilicate in the presence and absence of compatibilizer.

bilizer, respectively. In Figure 4, we clearly observe a relatively uniform and tight fractured surface of the BR nanocomposite containing the compatibilizer; the well-dispersed layered silicates are enclosed by the matrix and interlocked into the matrix phase. Very few voids, holes, and crack defects are present and no visible phase separation or craze propagation. In contrast, the fracture interface of the BR nanocomposite in the absence of the compatibilizer indicates that both phases possess relatively loose and phase-separated structures. In this image, we observe many cracks and voids and a crinkly disordered interface. From the FE-SEM and TEM results, we conclude that the blending of a polar organosilicate directly with a nonpolar BR must involve a compatibilizer as well as suitable process parameters if it is to generate a reinforced rubber nanocomposite containing well-dispersed layered silicates.

Mechanical Properties

Figure 6 presents the tensile stress–strain curves for BR nanocomposites containing different amounts of organosilicate and in the presence and absence of the compatibilizer. It is apparent that the BR nanocomposite displays the highest tensile strength and elongation when it incorporates both the organosilicates and the compatibilizers. In contrast, the nanocomposite containing only the organosilicate has relatively improved tensile strength and elongation than that of the neat BR. The nonpolar BR, which has a low surface energy, is not very compatible with the polar organosilicate. An amphiphilic compatibilizer having a structure similar to that of BR, but also having some polarity, is most suited to enhance the wettability and the interfacial interactions between the BR and the organosilicate. CTB, an oligomer that has both a slight polarity and a structure similar to that of BR, can move more rapidly into the intergallery spaces of the layered silicates than can the BR molecular chains, which leads to the entrance also of the intercalated BR molecular chains. We have found, however, that the BR nanocomposite containing both the organosilicate and the CTBN oligomer compatibilizer enhances the mechanical properties to a degree similar to that of the nanocomposite incorporating only the organosilicate. This finding may be due to the highly polar CTBN not being miscible with the nonpolar molecular chains of BR, which in turn reduces the interfacial interaction between the BR and the organosilicate, which even causes similar phase separation phenomena to those presented in Fig. 5. This phenomenon can be more easily understood as that of a conventional plasticizer, which softens the matrix, but reduces the tensile strength. The tear strengths presented in Fig. 7 follow the same trends as that of the tensile properties of those nanocomposites. We

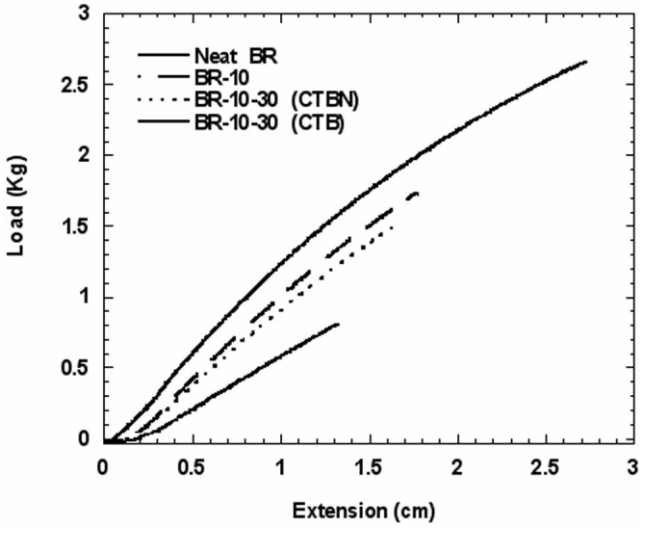

FIG. 7. Typical tear strength curves of the NBR nanocomposites containing 10 phr organosilicate in the presence and absence of compatibilizer.

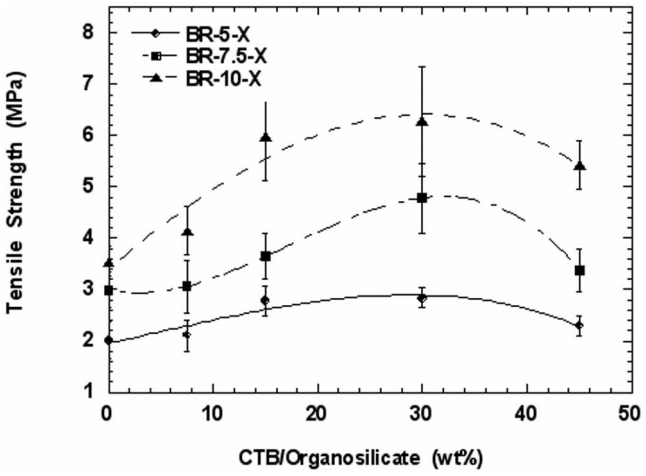

FIG. 8. The synergistic effect of the CTB/organosilicate ratio on the tensile stress–strain curves of the NBR nanocomposites containing various organosilicate contents (neat BR has a tensile strength of 201 ± 14 psi).

obtained significant improvements in the mechanical strength of the BR nanocomposites by using the melt blending method, followed by a vulcanization process, with the addition of a suitable compatibilizer. These results correspond to those observed in the FE-SEM images.

The mechanical properties of these nanocomposites increase upon increasing the amount of organosilicate and the relative loading ratio of CTB to organosilicate. Figures 8 and 9 display the materials' tensile strengths and tear strengths. The mechanical properties of the BR nanocomposites are enhanced relative to those of the neat BR because of the presence of the intercalated/exfoliated layered silicates. We obtained a more than four-fold increase in the tensile strength, a 150% increase in modulus at 100% elongation (M100), and 232 and 410% enhancements in the tear strength and elongation at

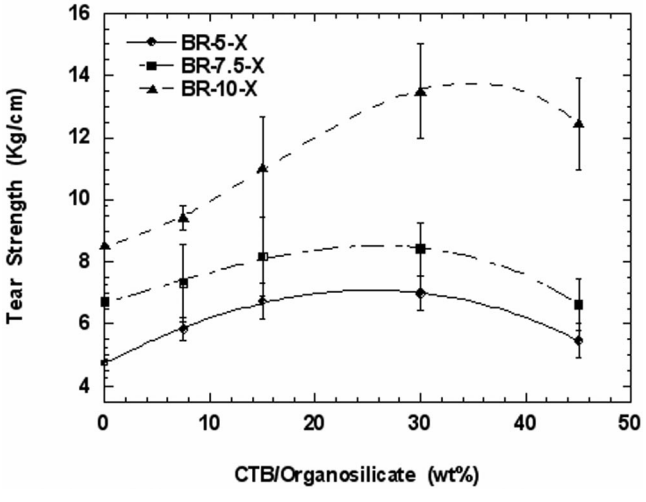

FIG. 9. The synergistic effect of the CTB/organosilicate ratio on the tear strength of the BR nanocomposites containing various organosilicate contents (neat BR has a tear strength of 22.83 ± 0.85 lb/in.).

TABLE 4. Crosslinking densities and thermodynamic characteristics of BR/organosilicate nanocomposites.

Sample	Volume fraction	Crosslink density (10^{-4} mol cm^{-3})	ΔG (J mol^{-1})	ΔS (J mol^{-1} K^{-1})
Neat BR	0.2025	1.152	−14.96	0.0494
BR-10	0.2010	1.131	−14.68	0.0484
BR-10–7.5	0.2094	1.250	−16.35	0.0540
BR-10–15	0.2080	1.230	−16.05	0.0530
BR-10–30	0.2067	1.210	−15.80	0.0521

break, respectively, upon the addition of 10 phr organosilicate and 3 phr CTB, relative to the corresponding values of neat BR. The enhancement in the mechanical properties and the gains in the elongation of these nanocomposites are quite different from those of conventional composites. The reinforcing effect is presumed to occur as a result of the intercalated/exfoliated organosilicate layers being covered by highly crosslinked elastomer molecular chains with a strong interfacial interaction between them [5, 13, 19]. The other effect may be the result of possible reactions of the ammonium salt intercalant and the zinc–sulfur–amine complex occurring between the organosilicate and BR during the vulcanization process; we have provided and discussed a similar reaction mechanism in a previous publication [31]. As a result, the BR molecular chains are more easily intercalated into the intergallery space of the organosilicate during this process.

We have also found that the mechanical properties improve upon increasing the loading ratio of CTB to organosilicate when it is below 30%, which is probably the upper limit of the loading ratio necessary to prepare intercalated/exfoliated elastomeric nanocomposites possessing outstanding mechanical properties. When the ratio increases above 30%, the mechanical properties decrease slightly.

The effect that the incorporation of the organosilicate has on the crosslinking density of BR can be estimated by using the Flory–Rehner equation. Table 4 summarizes the crosslinking density and thermodynamical characteristics of the BR compounds. The BR nanocomposites containing compatibilizers display higher crosslinking densities than do the other BR compounds. The crosslink density and the thermodynamic characteristics both reach plateaus at high CTB loadings, which indicate that exhausting of the cure agent by the compatibilizer occurs and leads to a slight decrease in the crosslink density. These results are in agreement with those of the vulcanization characteristics and the tensile properties, and indicate that a strong rubber/organosilicate interaction occurs in the nanocomposites. Table 4 lists the thermodynamic parameters, ΔG and ΔS, of the BR nanocomposites. We observe a relative increase in the free energy of the compatible BR/organosilicate nanocomposites, which we attribute to the improved compatibility among the BR, compatibilizer, and organosilicate phases. Therefore, the molecular chains of the BR can penetrate into

DOI 10.1002/pen

TABLE 5. Thermal properties of BR/organosilicate nanocomposites.

Sample	T_d (°C) at 5% weight loss	T_d (°C) at 50% weight loss	E' (10^9 Pa)	T_g (°C)	tan δ (E''/E')
Neat BR	426	510	0.073	−72	1.018
BR-7.5	359	557	0.359	−80	0.475
BR-10	394	561	1.530	−80	0.202
BR-10–7.5	406	522	2.330	−68	0.249
BR-10–15	406	523	2.227	−71	0.258
BR-10–30	409	519	1.961	−70	0.196
BR-10–45	423	519			

the galleries more easily to result in an intercalated/exfoliated structure.

Thermal Properties

We analyzed the thermal properties of the BR nanocomposites by using TGA. Table 5 summarizes the values of the degradation temperatures (*T*d). The 5% weight loss temperature decreased upon increasing the amount of organosilicate. This situation arose because the organo-modifier begins to decompose at temperatures above 200°C [20]. We chose the temperature at which 50% weight loss occurred to be the degradation temperature. As expected, the resistance to thermal decomposition improved upon the addition of the organosilicate, but it became weaker upon the addition of the low-molecular-weight CTB. The decomposition temperature of the nanocomposite containing a 10 phr loading of organosilicate (561°C) was 51°C higher than that of neat BR (510°C), but it increased only slightly (9–13°C) upon the addition of CTB.

Relaxation Behavior

The relaxation behavior of the nanocomposites is investigated by using DMA. The values of storage moduli (E'), glass-transition temperatures (T_g), and tan δ are also summarized in Table 5. The onset storage modulus (E') of the nanocomposite increased more with respect to the amount of organosilicate and the CTB-to-organosilicate loading ratio than did that of the neat BR. These results can be attributed to the larger active surface area and stronger BR–CTB–organosilicate interactions, and are consistent with the results of their mechanical properties (referred to Fig. 8), especially related to the tensile modulus (e.g., M100) from tensile test. We obtained the glass-transition temperature from the peak temperature of tan δ, as depicted in Table 5. Greater decreases in the values of T_g and tan δ—relative to those of the neat BR—also occurred as the organosilicate content increased. Similar results have been reported and rationalized for ammonium salts intercalated in silicate layers that may act as plasticizers or lubricants [19, 38]. When a compatibilizer is added, well-intercalated BR molecular chains can be led into the intergallery space of the layered silicate more readily and constructed more tightly; this process may constrain the mobility and flexibility of the alkylammonium salt and also result in increases in the values of the decomposition temperatures (5% weight loss), storage moduli (E'), glass-transition temperatures (T_g), and tan δ.

Barrier Properties

Figure 10 displays the improvement in the barrier to water vapor of the BR-based nanocomposites. The relative water vapor permeability of the BR nanocomposites reduced markedly (by 80%: from 100 to 20%); the permeability value for water in neat BR is 50.51 gm/m^2·day. This finding indicates that the intercalated/exfoliated BR/silicate nanocomposites improve the vapor barrier properties markedly. The permeability is controlled by the microstructure of the nanocomposite and by the interactions between the BR and the organosilicates. It seems that the compatibilizer has little effect on the water vapor permeability of the BR nanocomposites.

The marked enhancements we present in this study of the mechanical properties of the BR after forming nanocomposites through a two-stage melt blending process are quite attractive when compared to those of other rubber nanocomposites obtained when using the latex blending or solution or melt mixing processes that have reported in the

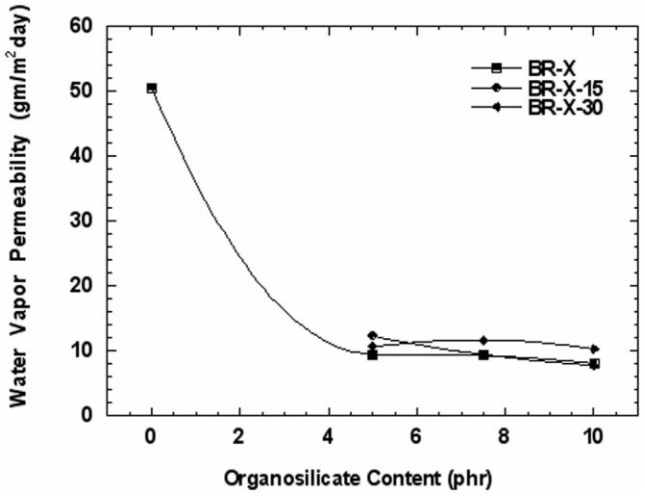

FIG. 10. Water vapor permeabilities of the BR nanocomposites containing various organosilicate contents.

literature [19, 31, 38, 39]. For example, using this method, we have achieved a four-fold increase in the tensile strength and the ultimate elongation. The thermal properties and the results of permeability tests indicate the same positive trends, which can be attributed to a number of factors. The first is that the interlayer distance of the layered silicate is expanded more by the CTB compatibilizer and a synergistic effect leads to better compatibility among the BR, compatibilizer, and organosilicate phases. Therefore, the BR molecular chains can penetrate into the galleries more readily and result in an intercalated/exfoliated structure [26, 30]. In addition, the number of agglomerated silicate particles is reduced significantly by the shearing force present during melt blending when using a suitable compatibilizer; this process also leads to the better dispersion and miscibility of the organosilicate in BR matrix.

CONCLUSIONS

We have successfully prepared BR/organosilicate nanocomposites that have intercalated and partially exfoliated structures by using a two-stage melt blending method. As a result of counteracting the polarity effect and compatibility effect, the tensile properties and tear strengths of these nanocomposites increase substantially—relative to those of the neat BR—upon increasing the amounts of incorporated compatibilizer and organosilicates that contain a low weight percent of layered silicates. We attribute these results to the significantly improved compatibility and the strong interactions among the polar layered silicates, compatibilizer, and nonpolar molecular chains of the BR. The BR molecules can interdiffuse into the intergallery space of the layered silicates more readily with the aid of the compatibilizer and result in an intercalated/exfoliated structure. Additionally, these nanocomposites exhibit higher thermal stabilities and dynamic storage moduli than those of the neat BR. The relative water vapor permeabilities of the BR nanocomposites containing 10 parts of organosilicate, both in the presence and absence of the compatibilizer, were reduced to 20% of that of the neat BR.

REFERENCES

1. K. Yano, A. Usuki, A. Okada, T. Kurauchi, and O. Kamigaito, *J. Polym. Sci., Part A: Polym. Chem.*, **31**, 2493 (1993).
2. D. Ratna, O. Becker, R. Krishnamurthy, G.P. Simon, and R.J. Varley, *Polymer*, **44**, 7449 (2003).
3. N. Salahuddin, A. Moet, A. Hiltner, and E. Baer, *Eur. Polym. J.*, **38**, 1477 (2002).
4. J. Fröhlich, R. Thomann, and R. Mülhaupt, *Macromolecules*, **36**, 7205 (2003).
5. A. Mousa and J. Karger-Kocsis, *Macromol. Mater. Eng.*, **286**, 260 (2001).
6. Z. Wang and T.J. Pinnavaia, *Chem. Mater.*, **10**, 1820 (1998).
7. T.K. Chen, Y.I. Tien, and K.H. Wei, *Polymer*, **41**, 1345 (2000).
8. H.L. Tyan, C.M. Leu, and K.H. Wei, *Chem. Mater.*, **13**, 222 (2001).
9. S. Varghese, J. Karger-Kocsis, and K.G. Gato, *Polymer*, **44**, 3977 (2003).
10. J. Ma, J. Xu, J.J. Ren, Z.Z. Yu, and Y.W. Mai, *Polymer*, **44**, 4619 (2003).
11. H. Zhao and D.A. Shipp, *Chem. Mater.*, **15**, 2693 (2003).
12. H.L. Tyan, K.H. Wei, and T.E. Hsieh, *J. Polym. Sci., Part B: Polym. Phys.*, **38**, 2873 (2000).
13. Y.I. Tien and K.H. Wei, *Macromolecules*, **34**, 9045 (2001).
14. Z. Wang and T.J. Pinnavaia, *Chem. Mater.*, **10**, 3769 (1998).
15. M. Ganter, W. Gronski, H. Semke, T. Zilg, C. Thomann, and R. Mülhaupt, *Kautsch. Gummi Kunstst.*, **54**, 166 (2001).
16. S. Joly, G. Garnaud, R. Ollitrault, and L. Bokobza, *Chem. Mater.*, **14**, 4202 (2002).
17. M. Krook, A.C. Albertsson, U.W. Gedde, and M.S. Hedenqvist, *Polym. Eng. Sci.*, **42**, 1238 (2002).
18. R.A. Vaia, H. Ishii, and E.P. Giannelis, *Chem. Mater.*, **5**, 1694 (1993).
19. W.G. Hwang, K.H. Wei, and C.M. Wu, *Polymer*, **45**, 5729 (2004).
20. Y.P. Wu, L.Q. Zhang, Y.Q. Wang, Y. Liang, and D.S. Yu, *J. Appl. Polym. Sci.*, **82**, 2842 (2001).
21. M. Janis, D.C. Brown, and R.A. Vaia, *Chem. Mater.*, **12**, 3376 (2000).
22. C.S. Triantafillidis, P.C. LeBaron, and T.J. Pinnavaia, *Chem. Mater.*, **14**, 4088 (2002).
23. T. Agag, T. Koga, and T. Takeichi, *Polymer*, **42**, 3399 (2001).
24. J.H. Park and S.C. Jana, *Macromolecules*, **36**, 2758 (2003).
25. R. Fayt, R. Jérôme, and P. Teyssié, *J. Polym. Sci., Part B: Polym. Phys.*, **27**, 775 (1989).
26. T.H. Chen, J.J. Zhu, B.H. Li, Z.Y. Yuan, P.C. Sun, Q.H. Jin, D.T. Ding, and A.C. Shi, Chinese patent ZL 02149126, 7, (2004)
27. C. Laurens, C. Creton, and L. Léger, *Macromolecules*, **37**, 6814 (2004).
28. M. Pluta, *Polymer*, **45**, 8239 (2004).
29. B. Yalcin and M. Cakmak, *Polymer*, **45**, 6623 (2004).
30. T.H. Chen, J.J. Zhu, B.H. Li, S.Y. Guo, Z.Y. Yuan, P.C. Sun, D.T. Ding, and A.C. Shi, *Macromolecules*, **38**, 4030 (2005).
31. W.G. Hwang, K.H. Wei, and C.M. Wu, *Polym. Eng. Sci.*, **44**, 2117 (2004).
32. M. Arroyo, M. López-Manchado, and B. Herrero, *Polymer*, **44**, 2447 (2003).
33. J. Karger-Kocsis and C.M. Wu, *Polym. Eng. Sci.*, **44**, 1083 (2004).
34. H.R. Dennis, D.L. Hunter, D. Chang, S. Kim, J.L. White, J.W. Cho, and D.R. Paul, *Polymer*, **42**, 9513 (2001).
35. M. Song, C.W. Wang, J. Jin, A. Ansarifar, Z.Y. Zhang, and M. Richardson, *Polym. Int.*, **54**, 560 (2005).
36. L.H. Sperling, *Introduction to Physical Polymer Science*, 2nd ed., Wiley, New York, Ch. 9, 382 (1993).
37. C.I. Park, O.O. Park, J.G. Lim, and H.J. Kim, *Polymer*, **42**, 7465 (2001).
38. Y.S. Choi, M.H. Choi, K.H. Wang, S.O. Kim, Y.K. Kim, and I.J. Chung, *Macromolecules*, **34**, 8978 (2001).
39. J.T. Kim, T.S. Oh, and D.H. Lee, *Polym. Int.*, **52**, 1203 (2003).

DOI 10.1002/pen